Contribution study of different common mode voltage sources on wind turbine main shaft bearing currents

Citation for the original published paper (version of record):
Zhao, J., Lei, X., Zhu, X. et al (2026). Contribution study of different common mode voltage sources on wind turbine main shaft bearing
currents. IEEE Access, 14: 107530-107545. http://dx.doi.org/10.1109/ACCESS.2026.3706131

Received 6 May 2026, accepted 7 June 2026, date of publication 24 June 2026, date of current version 20 July 2026.
Digital Object Identifier 10.1109/ACCESS.2026.3706131

RESEARCH ARTICLE

Contribution Study of Different Common Mode Voltage Sources on Wind Turbine Main Shaft Bearing Currents

JIAN ZHAO[1], XIAOFEI LEI[2], XULIANG ZHU[3], KEFEI ZHU[4,5], AND OLA CARLSON[1]
[1]Department of Electrical Engineering, Chalmers University of Technology, 412 96 Gothenburg, Sweden
[2]Department of Electronic and Information Engineering, Hulunbuir University, Hulunbuir 021008, China
[3]Department of Longli Wind Power Plant, CGN (Guizhou) New Energy Company Ltd., Guiyang 550081, China
[4]Shanghai Electric Drive Company Ltd., Shanghai 201800, China
[5]School of Mechatronic Engineering and Automation, Shanghai University, Shanghai 200444, China
Corresponding authors: Jian Zhao (zjian@chalmers.se) and Kefei Zhu (zhukefei@chinaedrive.com)

This work was supported by the research project ''Detecting and Eliminating Bearing Currents for Longer Lifespan of Main Shaft Bearings'' funded by Swedish Energy Agency under Grant 2017-008071/44949-1.

ABSTRACT Main shaft bearing failures in wind turbines have drawn increasing attention due to their high maintenance costs and operational risks. While previous studies have primarily focused on mechanical causes or bearing currents induced by generator-side common-mode voltage (CMV), limited attention has been given to other sources and system-level interactions. This paper addresses these gaps by presenting a unified modeling framework that captures CMV contributions from both the generator and the pitch system—each driven by pulse-width modulation (PWM) inverters. An equivalent capacitive circuit model is developed based on parasitic capacitances among key subsystems, including the generator, pitch motor, hub, shaft, and grounding paths. The bearing voltage ratio (BVR) is derived using the superposition principle to quantify the influence of each CMV source. The model accommodates different turbine configurations, such as geared and gearless systems, enabling analysis of architecture-dependent behaviors. Critical interface parameters are also identified and evaluated through sensitivity analysis. Experimental validation is conducted using a custom test platform and simulation model, confirming the accuracy of the proposed approach. The findings offer new insights into the role of different system CMVs in shaft voltage buildup and provide guidance for more effective design and mitigation strategies in wind turbine systems.

INDEX TERMS Wind energy, bearing currents, common mode voltage, impedance model, electrical drive, pulse width modulation.

I. INTRODUCTION

With the increasing global demand for sustainable energy and the need to reduce carbon emissions, wind energy has emerged as a key player in the transition to renewable power. According to the Global Wind Energy Council, global wind power capacity installed in 2025 had surpassed 1299 GW [1], underscoring the growing role of wind energy in global power generation. However, as wind turbines become larger and more complex, the reliability and maintainability of these systems have become critical concerns for both operators and researchers.

Among the various challenges faced by wind turbines, main shaft bearing failures have drawn increasing attention due to their rising frequency and associated maintenance costs. As the key mechanical link between the rotor hub and drivetrain, the main bearing plays a vital role in ensuring turbine performance and reliability. Unlike many other components, it is not easily accessible—particularly in offshore installations—making failures both difficult to detect and extremely costly to repair. These issues often result in extended downtime and substantial financial losses for operators [2], [3], [4].

The associate editor coordinating the review of this manuscript and approving it for publication was Feng Wu.

Conventional understanding suggests that main shaft bearing failures are primarily caused by mechanical issues such as excessive loading, misalignment, or lubrication failure [3], [5], [6], [7]. Nevertheless, recent studies indicate that electrical bearing currents may also play a significant role in accelerating wear and damage of bearings. Although these currents may not always serve as the root cause, they can lead to localized heating, electrical erosion, and fluting, thereby intensifying the degradation process of the bearing [8], [9], [10], [11], [12]. A clear understanding of these electrical mechanisms is therefore essential for enhancing turbine reliability and minimizing maintenance costs. Although bearing current issues in wind turbines have only recently received attention, they are not a new phenomenon in the broader field of electrical engineering. In fact, extensive research has already been conducted on bearing currents in various types of electrical machines (EMs), particularly those powered by pulse-width modulation (PWM) inverters. These inverters introduce high-frequency common-mode voltages (CMVs) into motor-drive systems, which in turn give rise to several types of bearing current phenomena, including capacitive discharge currents and circulating currents [13], [14], [15]. As a result, numerous mitigation techniques—such as shaft grounding, bearing insulation, and common-mode filtering—have been developed and successfully implemented in industrial applications [13], [16], [17].

Despite extensive research on bearing currents, most studies have concentrated on standalone motor systems, where the electrical and mechanical configurations are relatively consistent and predictable. In contrast, wind turbines incorporate a variety of interconnected subsystems—including the power generation system and transmission train (e.g., generator, main shaft, and hub), the pitch system, and the grounding system. These elements are coupled through complex parasitic capacitances, forming multiple paths for CMV propagation throughout the structure. Such complexity significantly affects the voltage distribution along the rotating shaft and contributes to the development of bearing currents. However, the influence of CMV on main shaft bearing currents in wind turbines has received limited attention in previous researches. Only study [18] has considered the generator-side CMV in a circuit model in geared wind turbine, leaving other system-level influences and other type wind turbines largely unexplored.

In wind turbine systems, common-mode voltage (CMV) is not solely introduced by the generator-side converter. Pitch systems, driven by PWM-based motors, also generate CMV that can couple into the main shaft and contribute to bearing currents. However, this influence remains largely overlooked, with limited understanding of its transmission paths or circuit-level impact on the main bearing.

Most existing studies focus on geared turbines, where generator-shaft decoupling simplifies the analysis. In contrast, direct-drive and hybrid systems present distinct structural and electrical characteristics, altering CMV behavior and its effect on bearing currents. The neglect of pitch system contributions and turbine diversity has left key gaps in current models and mitigation strategies.

To address this, a comprehensive system-level capacitive circuit model is proposed, capturing generator- and pitch-induced CMV interactions through parasitic capacitances between subsystems such as the generator, hub, pitch motor, main shaft, and grounding paths. Based on this, the BVR is derived using the superposition principle to quantify individual CMV source contributions across turbine types. The study further explores how configuration and interface parameters affect CMV propagation and bearing current risk, forming a foundation for targeted design improvements.

The paper is organized as follows: Section II reviews typical wind turbine architectures and introduces a unified model for general analysis. Section III presents the modeling of CMV propagation paths with equivalent circuits. Section IV defines and applies the BVR for quantitative assessment. Section V validates the model through simulations and experiments, and Section VI concludes with a summary and directions for future research.

II. MAIN SHAFT BEARING CURRENTS IN WIND TURBINES

In wind turbine systems, the main shaft bearing plays a crucial role in ensuring the stability and proper functioning of the drivetrain. Positioned between the turbine rotor and the nacelle frame, the main shaft bearing is responsible for supporting the weight of the whole turbine rotor. The main bearing is subject to both axial and radial loads, as well as cyclic stresses due to the varying forces exerted by the wind. As a result, the main bearing is typically designed with larger dimensions, often more than 50 cm in diameter [4], [6], [19], to handle these combined forces. To efficiently support both radial and axial loads, the main bearing is usually chosen as double-row roller bearings.

A. MECHANICAL & ELECTRICAL CONNECTIONS OF MAIN SHAFT BEARING

In order to investigate the main shaft bearing current issue effectively, it is essential to understand the installation position, mechanical connections, and the frequently neglected electrical connections associated with the main shaft bearing. These factors serve as the fundamental prerequisites for any analysis of bearing currents, as the electrical behavior of the system is closely linked to both its mechanical configuration and the underlying electrical connections.

Currently, wind turbines can be classified into two major categories: geared and gearless turbines [20], [21], [22]. The former utilizes a gearbox to reduce the torque required by the generator, thereby significantly decreasing its size, while the latter eliminates the need for a gearbox, allowing for a more integrated structural design. In order to study the electrical connection inside the wind turbine, the analysis is first conducted based on a geared wind turbine configuration.

In the typical geared wind turbine structure shown in Fig.1, the main shaft bearing is located within the nacelle. The rotating side of the bearing supports the main shaft, which connects to the hub frame, gearbox, slip ring, and ground disk. On one end, the main shaft is connected to the hub frame, a metal structure that supports the pitch system, while the other end serves as the low-speed input to the gearbox. The gearbox's high-speed output shaft is connected to the generator's input shaft through an insulated coupling. The stationary side of the bearing is securely fixed within the bearing housing. The bearing housing, gearbox, and generator are all mechanically attached to the metal nacelle frame. The nacelle is supported by the yaw system, which allows the turbine to adjust its orientation, and is connected to the metal tower structure. Finally, the tower is anchored to the ground through a concrete foundation. Importantly, earth electrodes are embedded beneath the ground, providing the grounding point for the entire wind turbine system.

The electrical connections that are concealed behind the mechanical interfaces play a critical role and must be carefully considered in the study of main shaft bearing currents. A thorough understanding of these electrical links is essential for accurately analyzing bearing current behavior. What should be emphasized is that the only electrical isolation connection in the system occurs at the coupling (shown in purple) between the high-speed output shaft of the gearbox and the generator input shaft. All other mechanical interfaces, however, involve direct metal-to-metal contact, creating continuous electrical pathways that may contribute to the formation of bearing currents.

From an electrical aspect view, the wind turbine sections at tower height are grounded via the metal nacelle frame, which is directly connected to the metal tower via the yaw bearing and a separate grounding cable in parallel. Both paths ultimately lead to the earth electrode embedded beneath the foundation.

Inside the nacelle, various components are grounded through either mechanical connections or independent grounding cables that connect to the nacelle's metal frame.

In the hub side, the pitch system's grounding is achieved through its mechanical installation, naturally creating an electrical connection with the main shaft. As for the main shaft itself, its grounding is established through a separately installed ground disk, which is connected to the nacelle frame via a brush, thereby completing the grounding loop.

However, due to the grounding method on the hub side, where the main shaft is grounded through its mechanical connection, the electrical potential of the main shaft becomes identical to that of the hub frame. In this grounding path, the connection between the ground disk and the ground brush is a dynamic frictional contact, which inherently has lower reliability compared to direct mechanical connections. As a result, some of the floating charges on the main shaft may flow to the nacelle frame through the main bearing and gearbox.

In this scenario, parallel grounding branches are formed between the ground disk/brush, the main shaft bearing, and the gearbox, with the main shaft potential serving as the common reference voltage potential. The current in each branch is determined by the impedance of its respective path.

B. MAIN SHAFT BEARING CURRENTS' SOURCES

In the last section, the installation and electrical connections of the main shaft bearing have been clarified. The generation of bearing currents is caused by the potential difference between the inner and outer rings of the bearing. Since the bearing housing ensures a reliable grounding connection through its mechanical installation, the variations in the potential of the main shaft become the driving force behind the formation of bearing currents. Consequently, the study of main shaft bearing currents' sources transforms into an investigation of the underlying causes of potential fluctuations on the main shaft.

A wind turbine consists of various subsystems, almost each of which relies on electrical power to operate. As a result, the turbine system contains numerous potential sources that could lead to the generation of bearing currents, especially in relation to the main shaft bearing. Based on the previous analysis, the investigation of bearing current sources can be focused on subsystems that are electrically connected, either directly or indirectly, to the main shaft.

As shown in Fig.1, the main shaft of the wind turbine is a metal hollow shaft. On the hub side of the shaft, the primary components include the pitch system and the wind turbine blades. On the drivetrain side, the main shaft acts as the input shaft for the gearbox, passing directly through the gearbox housing. At the rear end of the main shaft, a slip ring is installed to provide electrical power to the subsystems within the hub. At the gearbox output end, the electrical connection between the gearbox and the high-speed shaft is interrupted by an insulated coupling between the output shaft and the high-speed shaft.

Among the subsystems connected to the main shaft, only the pitch system and the generator are electrical active components. Both of these subsystems commonly utilize power electronics, which results in the presence of CMV. Previous studies have shown that CMV plays a decisive role in the bearing currents of modern electrical machines [7], [8], [9]. Therefore, the presence of CMV within the wind turbine system must be regarded as a significant factor in the analysis.

C. PITCH SYSTEM IN WIND TURBINES

With the development and application of wind power generation, wind turbine configurations have evolved significantly. Initially, fixed-speed wind turbines were predominant, but they have gradually been replaced by modern variable-speed turbines with pitch control.

Alongside these developments, pitch systems have also undergone continuous development, transitioning from early mechanical pitch control to hydraulic pitch systems and, ultimately, to the currently dominant electric pitch systems. A typical electric pitch system is illustrated in Fig.2.

The system consists of a pitch converter, a pitch motor, and a pitch gearbox on each blade. The converter regulates the operation of the motor, which drives a primary gear mounted on its output shaft. This primary gear engages with

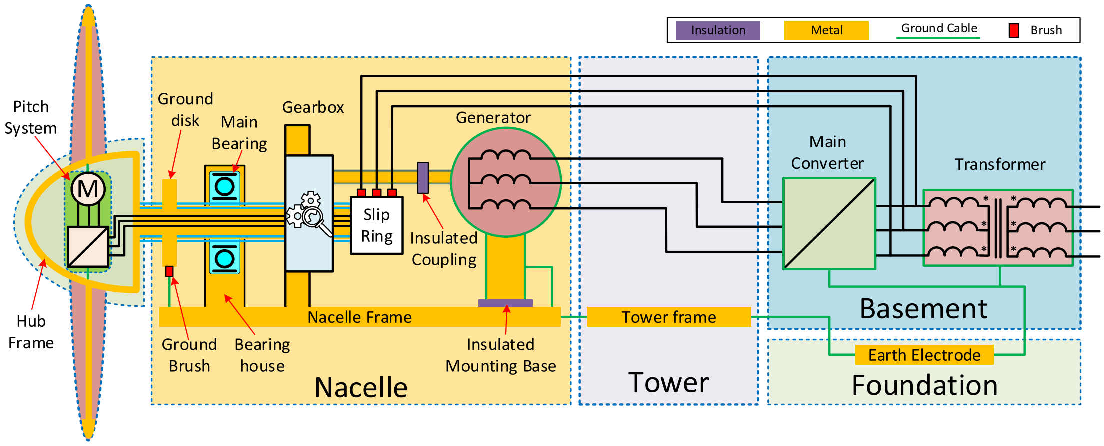

FIGURE 1. Electrical configuration of typical geared wind turbine.

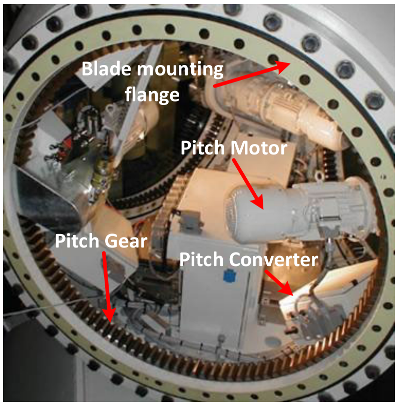

FIGURE 2. Configuration of typical electrical pitch system.

a secondary gear at the blade root, transmitting motion to adjust the blade pitch angle. By adjusting the pitch angle, the aerodynamic performance of the wind turbine can be effectively controlled. Furthermore, as shown in Fig.1, both the pitch motor and the pitch converter are mounted on the hub frame. The power supply for the pitch system is delivered directly from the grid side through the hollow main shaft and the slip ring installed at its rear end.

D. GENERAL CONFIGURATION FOR MAIN SHAFT BEARING CURRENTS STUDY

While the subsystems within the hub, particularly the electric pitch system and its installation, remain largely uniform across both geared and gearless wind turbines In gearless turbines, the main shaft is highly integrated into the generator, potentially allowing CMV from the generator to transfer directly into the main shaft. Consequently, a comprehensive analysis of main bearing currents requires a deeper investigation into the electrical configuration of gearless wind turbines.

A typical configuration of a gearless wind turbine is illustrated in Fig.3. Apart from the absence of a gearbox in the nacelle and the relocation of the slip ring to the rear end of the generator's main shaft, the remaining subsystems are identical to those in a geared wind turbine. In this configuration, the main shaft is directly integrated with the generator rotor. Unlike in geared turbines, the outer race of the main bearing is integrated with the rotating shaft, while the inner race is connected to the grounded bearing housing. As a result, the main bearing also functions as a bearing for the generator rotor, making the contribution of CMV from the generator windings a significant factor in the main shaft bearing currents.

To investigate the influence of CMV on main shaft bearing currents, it is essential to consider the distinct electrical and structural configurations of both geared and gearless wind turbines. This necessitates the establishment of a generalized configuration that incorporates the key characteristics of both turbine types, enabling a unified configuration for analysis. Fig.4 illustrates a specific type of gearless wind turbine, known as individual main bearing gearless wind turbine. In this configuration, the generator shaft serves as the main shaft of the turbine, consistent with conventional gearless designs. However, unlike typical gearless configurations, the main bearing is implemented as a separate unit and is mechanically mounted on the nacelle frame, consistent with the arrangement in geared wind turbines. Therefore, this configuration is adopted as the basis for analysis in this study, serving as a representative model for investigating main shaft bearing current mechanisms.

III. CMV'S TRANSMISSION PATHS

Building upon the conclusions drawn in Section II-B, it is identified that the two principal sources of CMV in a wind turbine system are the main generator windings and the electric pitch system. This section investigates the transmission mechanisms through which these CMVs couple to the main shaft, and analyzes their respective contributions to the formation of main shaft bearing currents.

A. CMV PATH ANALYZATION

Following the analysis presented in Subsection II-D, the wind turbine configuration illustrated in Fig.4 is selected as the

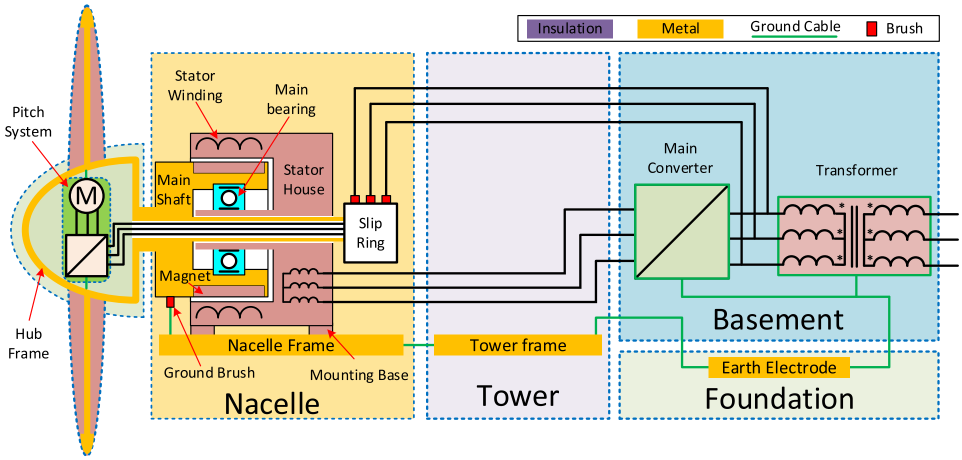

FIGURE 3. **Configuration of integrated bearing gearless wind turbine.**

representative configuration for this study. To account for both geared and gearless wind turbine architectures, an insulated coupling is conceptually introduced between the generator and the main shaft. This coupling, which is typically found only in geared wind turbines, is not present in actual individual bearing gearless wind turbines. Therefore, by switching between with or without the insulated coupling, the electrical behavior of both wind turbine types can be analyzed within a unified configuration shown in Fig.5.

As shown in Fig.5, components electrically connected to the main shaft include the main bearing, ground disk, generator, and the hub-mounted pitch system. Since the hub assembly is electrically floating, the shaft's potential can return to the grounded nacelle frame only via three paths: the ground disk, the main bearing, or the generator.

The shaft potential is primarily influenced by CMVs, among which the pitch system constitutes a significant source. In the pitch system, CMV is generated by the high-frequency switching operations of power electronic devices within the pitch converter and is transmitted via short cables to the windings of the pitch motor. Within the motor, multiple parallel leakage paths exist between the windings and the motor housing, which can be effectively modeled as a capacitive voltage divider [18]. For a given motor type, the ratio of CMV transferred from the winding to the housing remains approximately constant. Since the housing is directly bonded to the metallic hub frame, which is mechanically and electrically connected to the main shaft, the CMV present in the pitch motor windings is correspondingly coupled to the shaft in a fixed proportion. Accordingly, the transmission path of the pitch-induced CMV can be described as: pitch converter → motor winding → motor housing → hub frame → main shaft, as illustrated by the red dashed lines and arrows in Fig.5.

Additionally, it should be noted that the connection between the motor housing and hub frame may include non-metallic washers, which could introduce a capacitive effect rather than a direct low-resistance connection. This will be further discussed in the next subsection.

Another CMV source is the generator, where CMV originates from the high-speed switching of power electronics in the inverter. Unlike the pitch system, the inverter and generator are located separately, with a long cable running through the tower to deliver the CMV to the generator windings. In the generator, since the main shaft is integrated into the generator assembly, the transmission path of the CMV from the generator windings to the main shaft is more complex.

Since the generator is directly mounted onto the nacelle frame, its housing is effectively grounded. As a result, any CMV present on the main shaft within the generator can be conducted to ground through the generator bearings. Outside the generator, the CMV on the main shaft is further transmitted to the main bearing and ground disk.

Moreover, there exist multiple coupling paths between the generator windings and the grounded frame. Specifically, the CMV from the generator windings can reach the ground through the following routes:

Generator winding → Generator frame

Generator winding → Rotor (shaft) → Generator bearing → Generator frame

Generator winding → Rotor (shaft) → Main bearing / Ground disk

Among these three parallel paths, only the last one passes through the main bearing. Hence, in Fig.5, only this path is highlighted by green dashed lines and arrows to illustrate the transmission of generator CMV to the main shaft.

B. CMV TRANSMISSION CIRCUIT MODEL DERIVATION

In order to move beyond the qualitative analysis of CMV propagation paths presented earlier, it is necessary to establish a quantitative model. While the previous discussion focused on identifying these paths, understanding the specific impact of CMV on shaft bearing current requires more than topological insight. Based on the identified paths, a transmission circuit model must be developed to quantify this influence and determine the key contributing factors. This

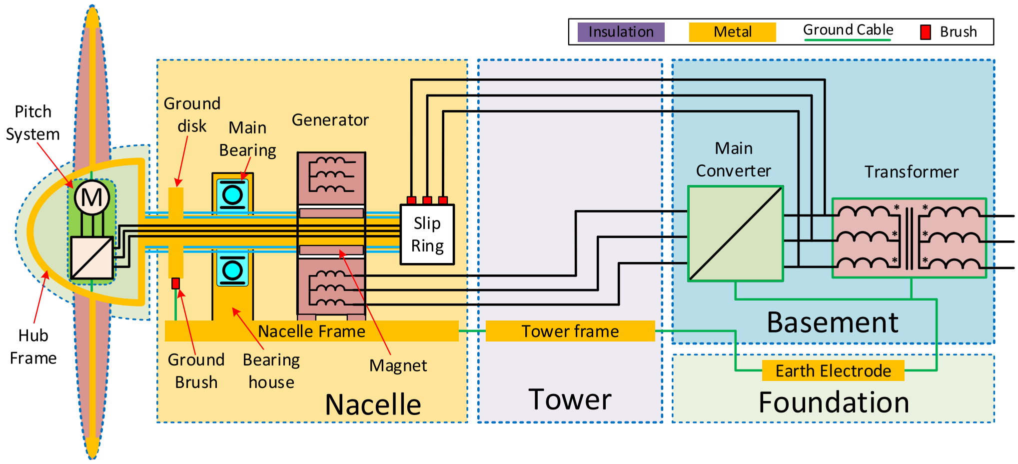

FIGURE 4. Configuration of individual bearing gearless wind turbine.

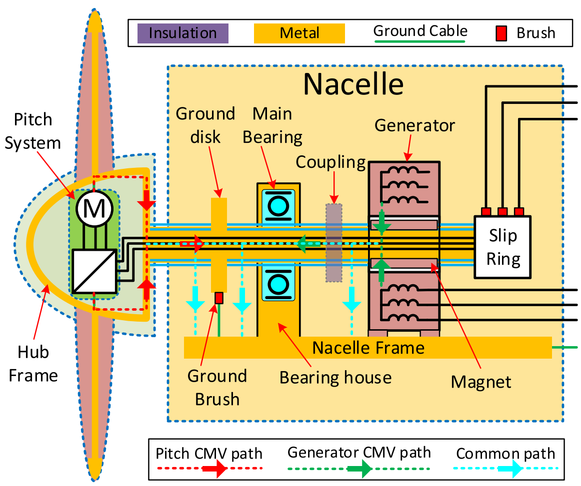

FIGURE 5. CMVs' transmission paths in wind turbine.

model enables a more detailed analysis of how different variables affect the magnitude of the bearing current.

1) ELECTRICAL MACHINE CMV PROPAGATION CIRCUIT MODEL

As previously analyzed, the origin of CMV in the system lies in the high-speed switching of converters, which generates voltage disturbances that propagate through cables to the windings of the electrical machine. However, the CMV that affects the main shaft bearing is ultimately originated from the electrical machine (motor/generator). Therefore, before developing the system-level circuit model, it is essential to review the internal transmission/coupling paths of CMV within the electrical machine.

Fig.6 illustrates the CMV propagation paths within the electrical machine. As reported in the literatures [11], [23], the CMV in the windings propagates via capacitive coupling between various internal components. The parasitic capacitances between these components are labeled in the cross-sectional view of the machine shown on the left side of the figure. Based on these capacitive relationships, a circuit model is derived to represent the CMV transmission paths among the windings, output shaft, and frame, as depicted in the light orange box on the right side of the figure.

The CMV refers to the potential difference between the winding neutral and ground. In wind turbine generator installation, the machine is grounded through its frame. In this case, the green dashed connection in the circuit model becomes solid, forming a closed grounding loop. Accordingly, two parallel coupling paths are formed between the winding neutral and the frame. One is through the capacitor C_{SWF}, which directly couples the windings to the stator and frame; the other path involves capacitive coupling from the stator to the rotor via C_{SWR}, and then from the rotor to the frame through the parallel combination of the rotor-frame capacitor C_{RF} and the bearing capacitor C_{BG}.

In the pitch motor installation, the pitch motor forms the grounding loop through the hub frame, the wind turbine main shaft ground disk, and the ground brush. In this case, the green dashed line in the circuit model on the right side of Fig.6 cannot be directly converted into a solid line anymore. Instead, a series of capacitors need to be added to represent the coupling relationships between the components along this path.

2) WIND TURBINE CMV PROPAGATION CIRCUIT MODEL

Based on the CMV distribution within the electrical machine discussed in the last section, as well as the installation configurations of both the pitch motor and generator shown in Fig.5, the circuit model can be further extended to represent the CMV propagation and distribution throughout the entire wind turbine system. The extended circuit model representing the system-level CMV propagation within the wind turbine is presented in Fig.7.

In the figure, the CMV distributions of the pitch motor and generator follow Fig.6 and are enclosed in dashed boxes matching the component colors from Fig.5. The hub and nacelle areas are similarly outlined for clarity.

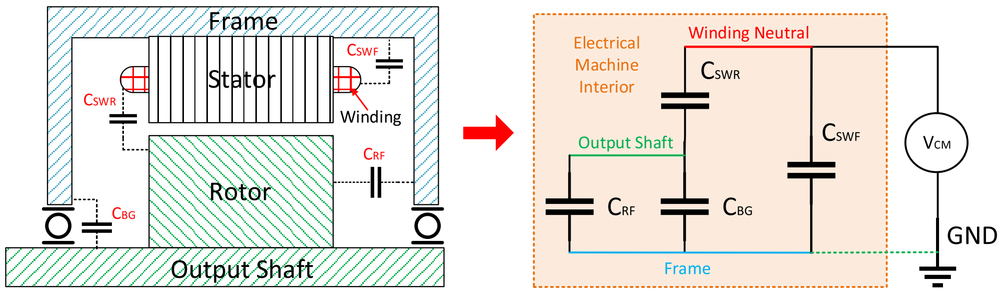

FIGURE 6. Electrical machine circuit model for CMV propagation study.

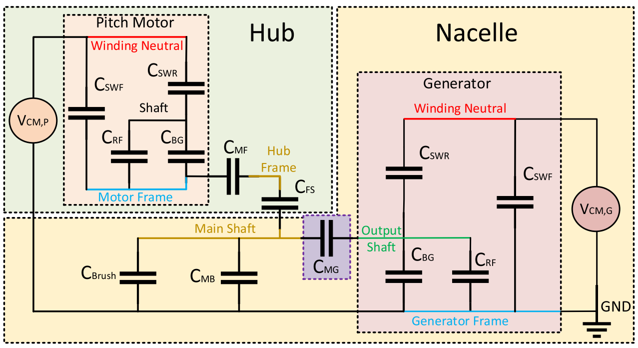

FIGURE 7. CMV transmission circuit model in wind turbine.

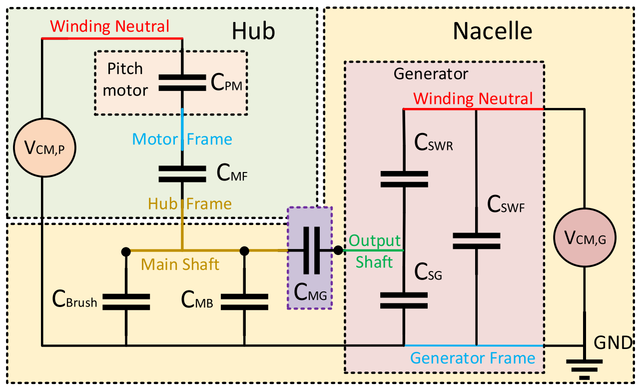

FIGURE 8. Simplified wind turbine CMV transmission circuit model.

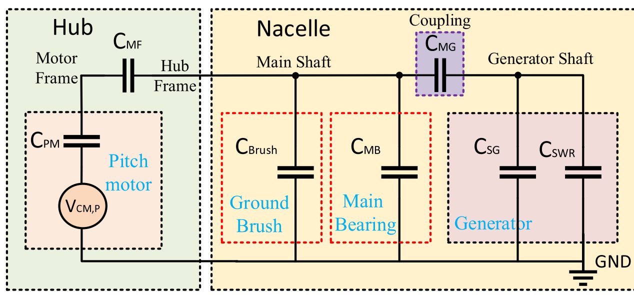

FIGURE 9. Pitch CMV transmission circuit model.

On the generator side of the circuit, grounding is achieved through its frame, making its circuit model consistent with that of a typical electrical machine. At its output end, the rotor shaft is electrically connected to the main shaft via the coupling's equivalent capacitance C_{MG}. The main shaft is grounded through two parallel paths: the shaft bearing capacitance C_{MB} and the equivalent capacitance of the grounding brush C_{Brush}.

On the pitch motor side, the configuration is more complex. The motor frame is connected to the hub frame via an equivalent capacitance C_{MF} at its mounting base. The hub frame is then coupled to the main shaft through the contact capacitance C_{FS} between them. From the main shaft to ground, the return path remains the same as on the generator side.

IV. CONTRIBUTION ANALYZATION AND KEY FACTORS

Targeting at analyzing the influence of CMV on main shaft bearing, this study takes a system-level perspective rather than focusing on individual components. Thus, based on the full circuit model in Fig.7, a simplified model is necessary to enable clearer analysis.

From the system point view, pitch CMV $V_{CM,P}$ enters the pitch motor via the windings and exits through its frame. Although the internal circuit involves multiple series and parallel capacitances, the entire pitch motor can be represented by an equivalent capacitance C_{PM}. Since the hub frame is directly connected to the main shaft, the contact capacitance C_{FS} can be neglected.

On the generator side, the rotor-frame capacitance C_{RF} and bearing capacitance C_{BG} form a parallel network and are simplified into a single equivalent capacitance C_{SG}. The simplified system-level circuit model is shown in Fig.8

A. BEARING VOLTAGE RATIO ANALYZATION

BVR is widely used in bearing current study in electrical machines [11]. It is defined as the ratio between the voltage across the bearing and the CMV, expressed as:

$$BVR = \frac{V_{Bearing}}{V_{CM}} \tag{1}$$

It reflects the ratio of the CMV couples to the bearing in electrical machines. A higher BVR indicates a greater proportion of CMV appearing across the bearing, which increases the risk of bearing current and potential electrical damage.

In the study of main shaft bearing currents in wind turbine systems, the concept of BVR can be extended from the motor-level to the system level. However, due to the increased complexity of the wind turbine system, a more

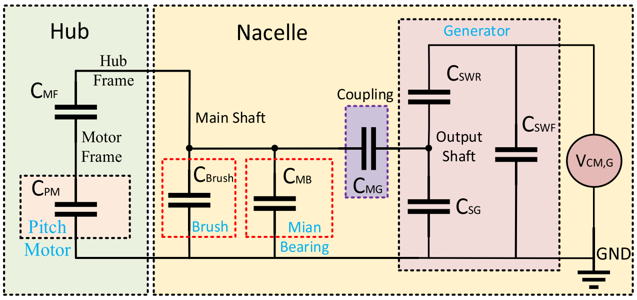

FIGURE 10. Generator CMV transmission circuit model.

detailed analysis of the main shaft bearing BVR becomes essential with the established circuit model. According to the superposition theory [24], [25], the two CMV sources in the circuit model (Fig.8) can be analyzed separately to determine their individual contributions to the main shaft bearing BVR.

1) PITCH CMV BVR DERIVATION

Starting with the pitch-side CMV, and applying the superposition theorem, the generator-side CMV is shorted. This isolates the effect of the pitch CMV, allowing for a focused analysis of its contribution to the main shaft bearing voltage. The corresponding simplified circuit model is shown in Fig.9.

Based on the simplified circuit, the potential on the main shaft can be derived. By applying Equation (1), the BVR contribution from the pitch-side CMV can then be calculated. The detailed derivation is presented as follows

$$V_{Bearing,P} = BVR_P \cdot V_{CM,P} \tag{2}$$

where,

$$BVR_P = \frac{(Z_{MG} + Z_{SG} \parallel Z_{SWR}) \parallel Z_{MB} \| Z_{Brush}}{(Z_{MG} + Z_{SG} \parallel Z_{SWR}) \parallel Z_{MB} \| Z_{Brush} + Z_{MF} + Z_{PM}} \tag{3}$$

2) GENERATOR CMV BVR DERIVATION

The analysis now turns to the contribution of the generator-side CMV. According to the superposition theorem, the pitch-side CMV is shorted in this case, leading to a simplified circuit model as illustrated in Fig.10.

Similarly, based on the simplified circuit model shown in the figure, the main shaft voltage and the corresponding BVR can be calculated, with the detailed derivation provided as follows.

$$V_{Bearing,G} = BVR_G \cdot V_{CM,G} \tag{4}$$

where,

$$BVR_G = \frac{[(Z_{PM} + Z_{FM}) \parallel Z_{Brush} \parallel Z_{MB} + Z_{MG}] \parallel Z_{SG}}{[(Z_{PM} + Z_{FM}) \parallel Z_{Brush} \parallel Z_{MB} + Z_{MG}] \parallel Z_{SG} + Z_{SWR}} \tag{5}$$

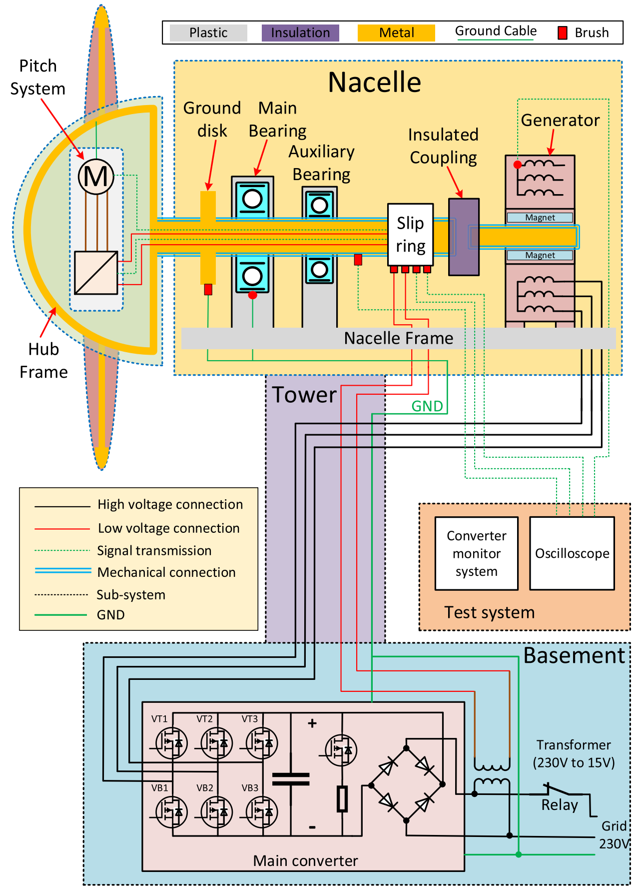

FIGURE 11. Lab turbine pitch system configuration.

B. DIFFERENT CMVS' CONTRIBUTION DISCUSSION

Continuing the previous analysis, the voltage across the shaft bearing in the actual system, where both CMV sources act together, can be obtained by superimposing the individual voltages contributed by each source. The expression for this is as follows:

$$V_{Bearing} = BVR_P \cdot V_{CM,P} + BVR_G \cdot V_{CM,G} \tag{6}$$

Since both BVR_G and BVR_P involve multiple capacitive elements—some constant and others variable—it is necessary to classify these capacitances. This classification enables a more structured analysis of the relative contributions of each voltage source and allows for the identification of the key factors influencing these contributions.

In wind turbine system design, key components such as the pitch motor, generator, and main shaft bearing are typically standardized commercial products. Consequently, the associated parameters—including C_{PM}, C_{SWR}, C_{SG}, C_{SWF}, and C_{MB}—can be regarded as constant values within the system. Although the main shaft bearing capacitance C_{MB} is theoretically a function of rotational speed, wind turbines generally operate within a narrow speed range. Therefore, C_{MB} can also be reasonably treated as a constant.

In contrast, parameters such as C_{MF}, C_{Brush} and C_{MG}, which are closely related to the physical installation and assembly quality of the turbine system, may vary across different turbines. These variables are the main focus of this study, as they directly influence CMV transmission and the resulting shaft bearing current. Specifically:

- $\boldsymbol{C_{MF}}$ represents the contact capacitance between the pitch motor and the hub frame. In some turbines, these components are in direct metal contact, resulting the $C_{MF} \rightarrow \infty$ ($Z_{MF} \rightarrow 0$). In other designs, a rubber vibration isolator is inserted between them, leading to a finite capacitance value.
- $\boldsymbol{C_{Brush}}$ denotes the contact capacitance between the grounding brush and the ground disk. Due to the rotational nature of the system, this capacitance is dynamic and influenced by several factors, including the relative speed between the brush and disk, material properties, contact area, contact pressure, surface roughness, and cleanliness. While some parameters—such as relative speed, material, and contact area—remain relatively stable over the turbine's lifecycle, others (e.g., pressure, cleanliness, and roughness) fluctuates with turbine operation, maintenance conditions, and even seasonal environmental changes, causing significant variation in C_{Brush}.
- $\boldsymbol{C_{MG}}$ refers to the coupling capacitance between the generator output shaft and the main shaft. In geared wind turbines, the coupling is often made of insulating materials such as glass or carbon fiber, electrically isolating the two shafts and resulting in $C_{MG} \rightarrow 0$, ($Z_{MG} \rightarrow \infty$). In gearless turbines, however, the coupling is usually metallic to meet mechanical strength requirements, making $C_{MG} \rightarrow \infty$, ($Z_{MG} \rightarrow 0$).

Due to the significant variation in C_{MG} across different turbines, a case-by-case analysis is required to accurately assess its influence on CMV transmission and bearing current behavior.

1) GEARED WIND TURBINE CASE

The following discussion begins with the geared wind turbine configuration $C_{MG} \rightarrow 0$ ($Z_{MG} \rightarrow \infty$). In this case, the CMV transmission path from the generator side is effectively blocked, and the shaft voltage is influenced solely by the pitch side $V_{CM,P}$.

$$V_{Bearing} = \frac{V_{Bearing} = BVR_P \cdot V_{CM,P} C_{MF} C_{PM}}{C_{MF}\left(C_{PM} + C_{MB} + C_{Brush}\right) + C_{PM}\left(C_{MB} + C_{Brush}\right)} \cdot V_{CM,P} \tag{7}$$

2) GEARLESS WIND TURBINE CASE

In the case of gearless wind turbine, $C_{MG} \rightarrow \infty$ ($Z_{MG} \rightarrow 0$),both $V_{CM,P}$ and $V_{CM,G}$ are active together. In wind turbine systems, the CMV generated by the pitch and generator subsystems are primarily determined by their respective supply voltages. The bearing voltage in a gearless wind turbine configuration can be achieved by equation (7). In this case,

$$BVR_P = \frac{C_{MF} C_{PM}}{C_{MF} C_{PM} + \left(C_{SG} + C_{SWR} + C_{MB} + C_{Brush}\right)\left(C_{MF} + C_{PM}\right)} \tag{8}$$

$$BVR_G = \frac{C_{SWR}}{\frac{C_{MF} C_{PM}}{C_{MF} + C_{PM}} + C_{SWR} + C_{SG} + C_{MB} + C_{Brush}} \tag{9}$$

As shown in Equations (8) and (9), the relative contributions of different CMV sources differ depending on the turbine configuration. A detailed assessment of these contributions requires consideration of several influencing parameters, comprising both constant and variable quantities. To facilitate further analysis, the numerical values of the constant parameters must be achieved, and the range of variation for the adjustable parameters must be defined. A more detailed discussion on parameter identification and subsequent analysis is presented in section V-C.

V. EXPERIMENTAL VERIFICATION

Building on the generalized wind turbine configuration and the CMV propagation analysis presented in Section III-B and IV, a circuit model was developed to investigate BVR and quantify the impact of different CMV sources on shaft bearing currents. The model also helped identify key factors influencing CMV coupling paths.

To verify the validity of the above analysis, testing on a real wind turbine would be ideal. However, due to the system complexity and safety requirements, such tests are challenging, and some subsystems are even inaccessible. Additionally, the generalized configuration shown in Fig.5 introduces an insulated coupling between the main shaft and generator, which does not exist in actual turbines.

Therefore, a simplified wind turbine setup is constructed under laboratory conditions. This setup does not replicate the full turbine structure, but includes only those subsystems directly relevant to the generation and transmission of shaft bearing current.

A. LAB SETUP DESIGN

Based on the design requirements outlined above, a downsized prototype wind turbine was constructed for experimental validation, as shown in Fig.11. Structurally, it consists of three main components: the tower, nacelle, and hub. Functionally, the configuration integrates a power generation system and an electrically driven pitch system. In addition, a dedicated monitoring subsystem is incorporated specifically to enable precise observation and analysis of the electrical phenomena associated with main shaft bearing currents. In the following subsections, the design and implementation of each subsystem within the prototype wind turbine are presented in detail.

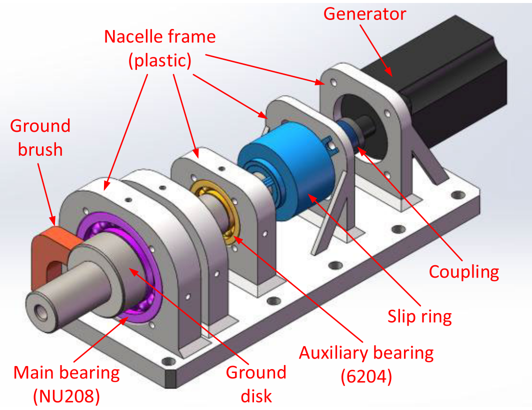

FIGURE 12. Lab turbine nacelle& power train prototype.

1) LABORATORY TURBINE MECHANICAL STRUCTURE

The experimental wind turbine with configuration in Fig.11 has a central height of approximately 80 cm. The structure is divided into three main sections: the tower, nacelle, and hub. The tower is constructed from a multi-layer wooden framework, with the main converter of the power generation system and a transformer for the pitch system installed in the basement layer. Thin metal sheets are used to cover the tower externally, imitating the metallic enclosure of a real wind turbine.

The nacelle is shown in Fig.12, it features a 3D-printed plastic frame, with wires connecting various metal components for easy monitoring of the turbine's operating status, which will be detailed in the monitoring system section. To ensure proper alignment with the generator and stable support for the main shaft, two bearings are employed: a cylindrical roller bearing (NU208) and a deep groove ball bearing (6204).

The roller bearing, which closely resembles those used in actual wind turbines, is the focus of this study, while the ball bearing is primarily responsible for supporting axial loads. To ensure that the deep groove ball bearing does not influence the study, its electrical behavior is isolated. This is achieved by the insulating properties of the nacelle's plastic structure, which keeps the ball bearing electrically floating, preventing any electrical loop formation.

Regarding the hub, since the blades do not affect the CMV's impact on the main shaft bearing current, the hub only contains the pitch system, which will be further detailed in the pitch system section.

2) POWER GENERATION SYSTEM

The power generation system consists of a permanent magnet synchronous generator (PMSG), its dedicated converter, and a hollow steel main shaft. The main shaft is connected to the generator rotor via an interchangeable coupling. To accommodate both geared and gearless configurations, the system allows for switching between an insulated coupling (for emulating geared turbines) and a metallic coupling (for gearless turbine scenarios).

Due to the absence of aerodynamic torque input blades, the PMSG operates solely in motor mode under laboratory conditions. However, as the focus of this study is on the CMV and its propagation paths, rather than the direction of energy flow, this operational mode does not affect the validity of the CMV analysis.

3) PITCH SYSTEM

The pitch system, consists of the pitch motor, pitch converter, a dedicated transformer for power supply, and a slip ring for electrical transmission. Due to the absence of blades, actual pitch operation cannot be implemented on the downscaled lab turbine. However, this study focuses on the transmission path of CMV generated by the pitch system. A brushless DC motor and its controller are used to emulate this behavior. The mechanical installation and electrical configuration of the pitch system are designed to be consistent with those of a real wind turbine, ensuring an accurate representation of CMV transmission. The configuration of the lab turbine's pitch system is illustrated in Fig.13.

The lab turbine power supply system is designed to replicate the one in an actual wind turbine. The power is drawn from the grid through a transformer, then transmitted via long cables to a slip ring mounted on the main shaft. From there, the power passes through the rotor of the slip ring, travels through the hollow shaft, and is delivered to the pitch rectifier installed on the hub, which rotates with the main shaft.

It should be note that the power supply voltage for the lab turbine's pitch system differs from that of an actual wind turbine. In real wind turbines, the pitch system is powered by 230VAC, while the generator side is 690VAC or higher. Since the lab system can only connect to a standard 230VAC power supply, which is much lower than that in actual wind turbines, the supply voltage to the pitch system had to be reduced. Taking both electrical limitations and safety considerations into account, the pitch system in the lab turbine operates with a lowered voltage of 15 VAC.

Aiming at increasing the current flowing through the pitch motor, three small resistors connected in a Y-configuration are placed in parallel with the motor windings. For structural compactness, the entire hub is implemented as an integrated PCB, as shown in Fig.14, with the rectifier, converter, pitch motor, and power resistors all mounted on it.

As shown in the side view of Fig.14c, two additional layers are positioned beneath the main PCB. One is the insulating board, and the other is a metal plate used to emulate the hub frame. The insulating board electrically isolates the PCB from the metal plate, except at the mounting point of the pitch motor frame, which is secured to the metal plate with metal screws.

These three layers are stacked axially to form the pitch system structure within the hub. The entire assembly is fixed to the main shaft via a threaded connection at the shaft's front end, where the metal plate is in direct face to the main shaft. Through this sandwich-style structural arrangement and installation method, the lab pitch system effectively

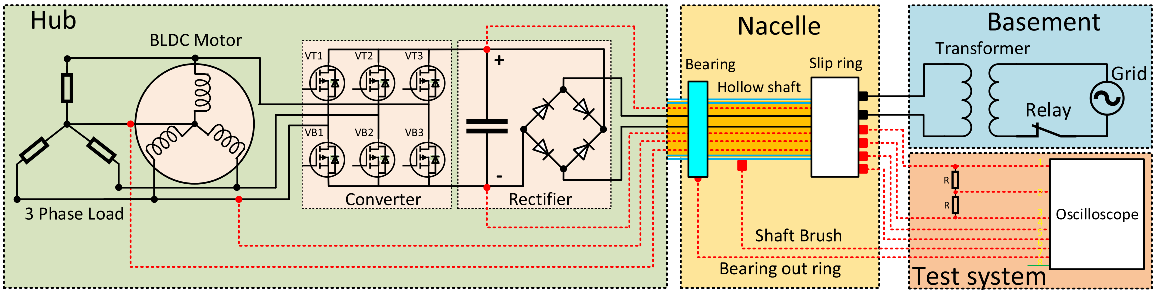

FIGURE 13. Lab turbine pitch system configuration.

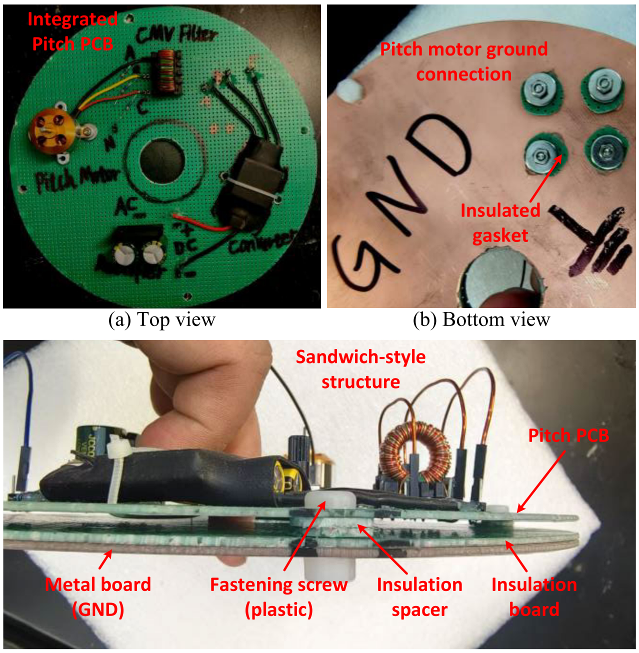

(a) Top view (b) Bottom view

(c) Side view

FIGURE 14. Lab turbine hub &pitch system prototype.

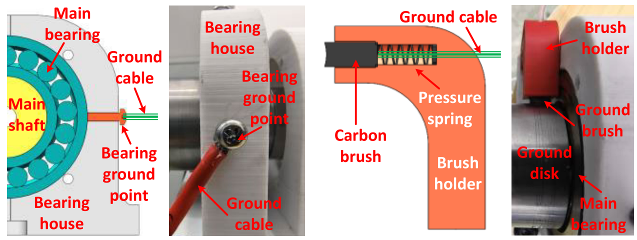

(a) Bearing ground (b) Shaft brush

FIGURE 15. Lab turbine monitor system signal collection point.

replicates the electrical connectivity of the pitch system in a real wind turbine.

4) MONITOR SYSTEM & SYSTEM GROUND

In real wind turbines, the monitoring system is designed to observe the overall operational status of the turbine. In contrast, the monitoring system in the lab turbine is specifically tailored for the investigation of CMV and main shaft bearing currents. Therefore, its primary function is to measure and record electrical signals relevant to CMV transmission and shaft current behavior. The configuration of the monitoring system in the lab turbine is illustrated by light orange block in Fig.11 and Fig.13, consisting primarily of an oscilloscope and multiple signal probes.

To support effective signal acquisition for CMV and shaft current analysis, the ground system of the lab turbine is redesigned. The goal is to maintain consistency with real wind turbine grounding while ensuring measurement accessibility. This is achieved by electrically isolating major components using the previously described plastic nacelle frame. Subsequently, their grounding points are reconnected via short copper wires. These wires serve not only as grounding paths but also as convenient locations for inserting signal probes, allowing accurate measurement without affecting the system's electrical behavior.

The main electrical signals monitored in the system include: the CMV at the winding neutral of the pitch motor, the DC-link voltages (+/−) at the converter input, the main shaft bearing current, and the shaft voltage. For the pitch-related signals, dedicated measurement points were reserved on the hub PCB during its design. These signals are conducted out via separate channels in the slip ring.

The outer ring of the main bearing is clamped within the bearing housing by screws, and one of these screws is connected to ground via a dedicated wire (as shown in Fig.15 a). The main shaft bearing current is measured by inserting a shunt resistor in this grounding path, converting the current into a voltage signal. The shaft voltage is captured using a spring-loaded brush pressed directly against the shaft surface, as illustrated in Fig.15b.

B. PARAMETER ACQUISITION

In order to further explore the analytical framework discussed in section IV-B, it is essential to obtain the constant values and variation ranges of the parameters defined in the model equations. Accordingly, this section focuses on extracting key electrical parameters—specifically C_{SWR}, C_{SG}, C_{PM}, C_{MB}, C_{Brush}, and C_{MF}—from the experimental platform illustrated in Fig.16.

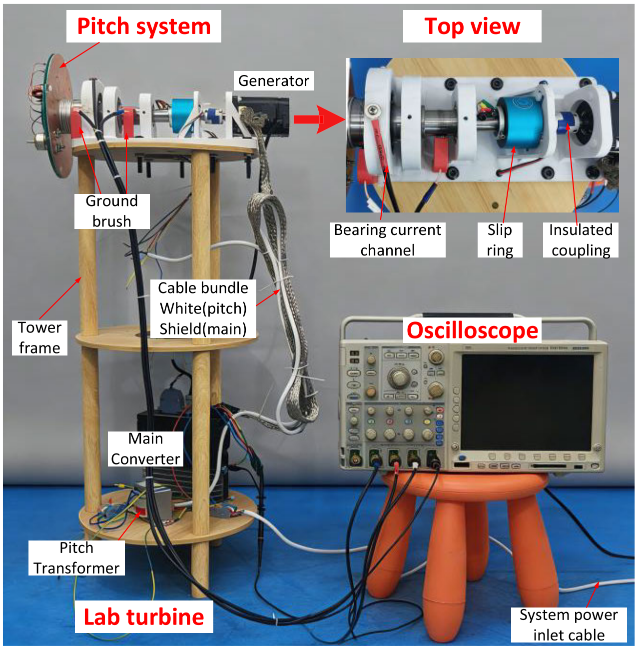

FIGURE 16. Lab turbine prototype.

TABLE 1. Lab turbine tested parameter.

Parameter	Value	Test condition
C_{SWR}	912 pF	Generator winding to house
C_{SG}	8.75nF	Generator bearing @100rpm
C_{PM}	144 pF	Pitch motor winding to house
C_{MB} @100rpm	314 pF	lithium-based grease $\varepsilon_r \approx 2.78$
	∞	Carbon conductive grease $\rho_v \approx 63\Omega\cdot$cm
C_{Brush} @100rpm	∞	Tight contact
	1.5 nF	Normal contact
	23.4 pF	Grease contaminated interface
C_{MF}	∞	Pitch motor direct contact mounting
	38.0 pF	Single insulated gasket spaced
	33.5 pF	Three insulated gasket spaced

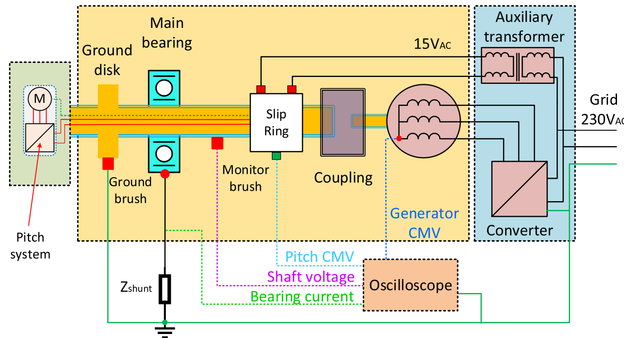

FIGURE 17. Lab test connection and signal detection.

For the static capacitances C_{SWR}, C_{SG}, and C_{PM}, their value are relative constant after assembling of the system. Thus direct measurements were performed using an LCR meter under 2 V, 5 kHz excitation

For the bearing capacitance C_{MB}, which is speed-dependent, the generator was first driven in motor mode, after which the main shaft was accelerated to 100 rpm to emulate the representative operating speed of a utility-scale wind turbine. Under this condition, C_{MB} was measured multiple times and the average value was recorded. Due to the smaller bearing size in the test rig, the lower roller line speed failed to establish a sufficient lubricant film, causing the bearing to remain in a conductive state. Aiming at replicating the insulated state observed in real wind turbine bearings, additional grease was applied to the test bearing to ensure similar dielectric behavior.

The brush contact capacitance C_{Brush}, which is installation-dependent, was characterized by varying the spring pressure and surface roughness at the brush–ground disk interface. Additionally, to emulate poor maintenance scenarios in actual turbines—where grease may contaminate the brush-to-ground disk interface—a test condition was introduced in which grease was deliberately applied to the contact surface.

For the pitch motor installation interface capacitance C_{MF}, different capacitance values are obtained by inserting various numbers of insulating spacer between the motor foot and the hub frame, as illustrated in Fig.14b.

The measured values of the above capacitances under various test conditions are summarized in Table 1.

The measurement results show that C_{SWR}, C_{SG}, and C_{PM} remain stable, while C_{MB}, C_{Brush}, and C_{MF} vary significantly with contact conditions. Under well-contacted or conductively filled states, these capacitances physically vanish; however, for mathematical analysis, they are approximated as $C \to \infty$.

Notably, C_{Brush} involves dynamic contact and does not achieve ideal conduction even under normal conditions. It instead exhibits capacitive behavior with relatively large capacitance (low impedance). When grease contamination is present, the capacitance decreases, resulting in a more pronounced capacitive behavior with higher impedance.

C. SYSTEM VERIFICATION

With the capacitance parameters of all subsystems and components obtained from the measurements, a simulation model is established based on the circuit structure shown in Fig. 8. Using Equations (7) and (9), this model enables a systematic evaluation of the contributions of different CMV sources to the resulting bearing voltage. To further validate the analytical and simulation results, comprehensive experimental verification is subsequently performed on the laboratory-scale turbine platform, with the corresponding experimental connections illustrated in Fig. 17.

The physical quantities measured in the experimental system include the bearing current $I_{Bearing}$, the shaft voltage $V_{Bearing}$, and the common-mode voltages on the generator and pitch sides, $V_{CM,P}$ and $V_{CM,G}$, respectively.

Direct measurement of the bearing current in the laboratory turbine is difficult because the system voltage is low and the

TABLE 2. Test case number definition.

Normal grease C_{MB}=314pF			
C_{Brush} / C_{MF}	Tight brush	Normal brush	Greased brush
Direct contact	Case 1	Case 2	Case 3
Three spacer	Case 4	Case 5	Case 6
Conductive grease $C_{MB}\to\infty$			
C_{Brush} / C_{MB}	Tight brush	Normal brush	Greased brush
Direct contact	Case 7	Case 8	Case 9
Three spacer	Case 10	Case 11	Case 12

resulting current is very small. This makes direct current sensing prone to large errors. To overcome this, a shunt resistor is placed between the bearing housing and ground. Its resistance is chosen to approximate the grounding resistance of a real turbine bearing house. $I_{Bearing}$ is then obtained by measuring the voltage across the shunt, which provides a more reliable signal.

The shaft voltage $V_{Bearing}$ is measured by installing an additional brush parallel with the ground brush, and ensuring a stable and low-impedance electrical contact by strong spring pressure on the additional brush.

The pitch-side CMV $V_{CM,P}$ is obtained by directly accessing the neutral point on the pitch PCB and routing the signal through the slip-ring signal channel. In contrast, the generator-side CMV $V_{CM,G}$ is measured directly from the neutral point of the PMSG stator windings.

Since geared and gearless turbines differ mainly in whether the PMSG is electrically connected to the main shaft, two coupling conditions are tested: an insulated coupling and a metallic coupling of identical size, representing the isolated and conductive cases. The following sections discuss these two configurations separately.

1) GEARED WIND TURBINE CASE($C_{MG}\to 0$, $Z_{MG}\to\infty$)

In geared case, the use of an insulating coupling electrically isolates the generator shaft from the main shaft, thereby blocking $V_{CM,G}$. Consequently, only the pitch-side common-mode voltage $V_{CM,P}$ is present.

Since different combinations may occur for the brush, bearing and the pitch motor installation, both simulation and experimental analyses were performed for various combinations of these states, as summarized in Table 2.

The waveform comparison under typical operating conditions is shown in Fig. 18. The color definitions of the oscilloscope channels are consistent with those in Fig. 17.

In Case 1, with the brush firmly pressed, both the V_{shaft} and current exhibit near-zero average values. Meanwhile, synchronous transient spikes are observed in both voltage and current waveforms.

In Case 2, corresponding to normal operating conditions, V_{shaft} follows a waveform trend similar to the pitch-side CMV. In the shaft current, *dv/dt* -induced current spikes appear at voltage transitions.

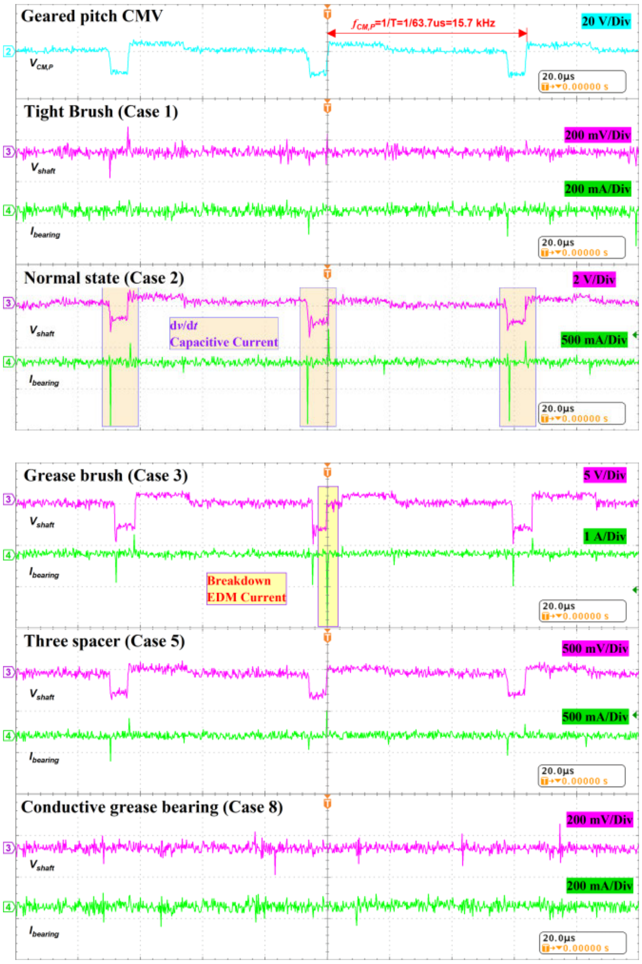

FIGURE 18. Lab turbine geared case test result comparison.

Comparing Case 2 and Case 3, when grease contamination is present on the shaft grounding brush, V_{shaft} increases significantly. In addition to the *dv/dt* current, oil film breakdown occurs in the bearing, resulting in high-amplitude EDM currents.

Comparing Case 2 and Case 5, after inserting insulation spacer between the pitch motor frame and the hub frame, V_{shaft} is substantially reduced. The bearing current contains only weak *dv/dt* components, with no EDM current.

In Case 8, when conductive grease is applied, the results are similar to Case 1 with a firmly tight brush. The stepped voltage waveform disappears, and only minor spikes and current transients are observed during switching events.

For the BVR analysis, a simulation model is established based on Fig. 8 using the parameters listed in Table 1. In both simulation and experimental results, the voltage values are extracted from the plateau regions of the stepped waveforms. According to the definition of *BVR* in equation (1), the corresponding BVR_P for each case is calculated. The results are summarized in Fig. 19.

A comparison of *BVR* across different cases shows that, in the tight brush conditions (Case 1/4/7/10) and when

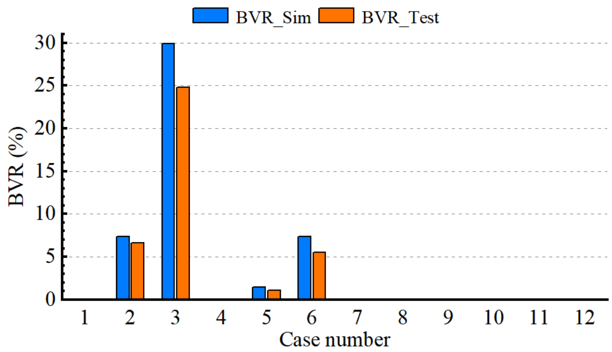

FIGURE 19. Lab turbine geared case BVR simulation vs test.

conductive grease is applied (Case 7–12), the *BVR* approaches zero (below 0.5% in both simulation and measurement).

From the quantitative results of BVR_P, the simulation and experimental data exhibit consistent trends. Comparing Case 2 and Case 3, the presence of grease increases BVR_P from approximately 6% to 25%. In contrast, comparisons between Case 2/5 and Case 3/6 show that introducing insulated spacers significantly reduces the CMV coupled to the main shaft by about 80%.

Comparing the simulation and experimental results for Case 2/3/5/6, the measured BVR_P values are consistently lower than the simulated ones, regardless of whether grease is present on the brush. This discrepancy can be attributed to the C_{Brush} values in Table 1, which are obtained under dynamic but short-duration conditions. In actual operation, longer rotational periods lead to smoother brush surfaces due to friction and more uniform grease distribution within the interface. As a result, a thinner and more stable air/oil film (with smaller gap) is formed between the brush and the shaft, leading to an increased C_{Brush} and consequently a reduced BVR_P according to equation (8).

2) GEARLESS WIND TURBINE CASE($C_{MG} \to \infty$, $Z_{MG} \to 0$)

In the gearless turbine configuration, the insulating coupling in Fig. 16 is replaced by a metallic coupling. In this case, it can be mathematically approximated that $C_{MG} \to \infty$ ($Z_{MG} \to 0$).

Under this condition, both $V_{CM,P}$ and $V_{CM,G}$ are active simultaneously, leading to a more complex interaction. As a result, BVR_P and BVR_G can no longer be evaluated independently, and a comprehensive analysis based on the measured waveforms is required. Similar to the geared turbine case, different operating conditions are defined based on brush contamination and the presence of insulation spacers in the pitch motor. The cases are indexed according to Table 2, and the corresponding waveforms are presented in Fig. 20.

From the experimental results, a similar trend to the geared turbine is observed. Under tight brush and conductive grease conditions (Case 1 and Case 8), the shaft voltage and current exhibit near-zero average values, with only transient spikes occurring during switching events. However, compared to

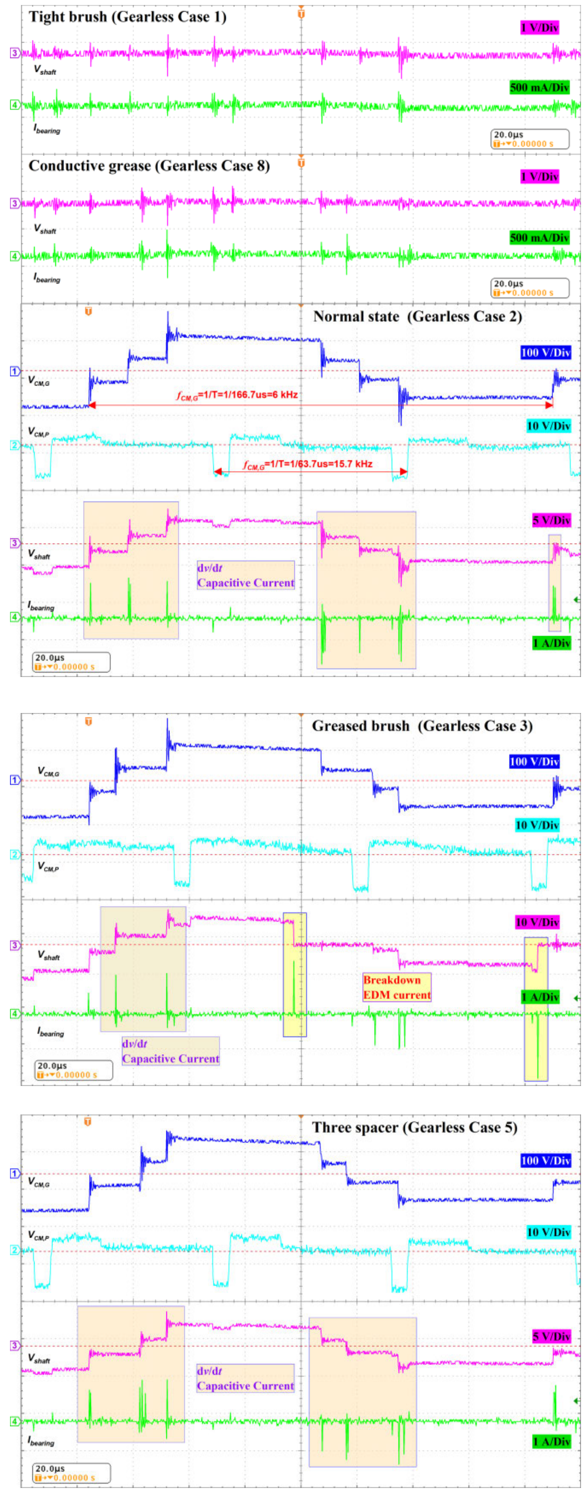

FIGURE 20. Lab turbine gearless case test result comparison.

Case 1 and Case 8 in the geared turbine (Fig. 18), the spike amplitudes are more than doubled. This is because the generator-side CMV is directly coupled to the main shaft through the metallic connection. Given that its magnitude is several times higher than $V_{CM,P}$, its impact is more direct and pronounced.

In Case 2/3/5, the generator-side CMV $V_{CM,G}$ exhibits the typical stepped waveform, with significant voltage overshoots occurring at the step transitions. The main shaft voltage waveform is dominated by the influence of $V_{CM,G}$, with $V_{CM,P}$ superimposed at a smaller proportion, due to the much larger magnitude of $V_{CM,G}$ compared to $V_{CM,P}$.

The bearing current waveform is primarily generated at the voltage transition moments of both $V_{CM,G}$ and $V_{CM,P}$, producing dv/dt-induced currents. Notably, the current amplitudes are largest at the transitions of $V_{CM,G}$.

In terms of voltage amplitude across different cases, V_{shaft} reaches its highest value in the greased brush Case 3, while Cases 2 and 5 show comparable amplitudes. Comparing Case 2 and Case 5, adding an insulation spacer slightly reduces the contribution of $V_{CM,G}$ to V_{shaft}. However, since the overall contribution of $V_{CM,G}$ is already low, the effect of the insulated spacer is limited.

In the greased brush Case 3, two bearing breakdown events were observed. After each breakdown, the shaft voltage dropped to zero and remained there until the voltage polarity reversed, at which point V_{shaft} resumed following the trend of $V_{CM,G}$. The breakdown was accompanied by large EDM current spikes.

It is important to note that bearing breakdown is influenced by multiple parameters and occurs probabilistically. As the voltage increases beyond a certain threshold, the likelihood of breakdown rises sharply. For example, in the geared turbine Case 3 (Fig. 18), only one breakdown waveform was captured in tens of tests, whereas in the gearless turbine Case 3, breakdowns were observed after just a few tests. Therefore, in Fig. 20, although V_{shaft} amplitudes in Case 2 and Case 5 are similar to those of Case 3 in Fig. 18, no breakdown occurred.

D. TEST RESULT DISCUSSION

Based on the above experimental results, the following observations can be made for both geared and gearless turbines:

- Tight brush contact and the use of conductive grease can effectively reduce BVR_P and BVR_G. However, *dv/dt*-induced current spikes during switching events still persist.
- A greased brush significantly increases the shaft voltage, leading to a much higher probability of bearing breakdown. In this case, the contribution of $V_{CM,P}$ increases by approximately four times, while that of $V_{CM,G}$ increases by about one time.
- Introducing an insulation spacer at the pitch motor grounding interface effectively reduces the influence of $V_{CM,P}$ on the shaft voltage, with a reduction of about 80%.

It should be noted that in the laboratory turbine, the pitch system voltage level (15 V) is much lower than that of the main power system (230 V), resulting in a relatively smaller contribution in the gearless configuration. In practical wind turbines, however, the pitch system typically operates at around 400 V, while the main power system is approximately 690 V. As this gap is significantly smaller than in the laboratory setup, the contribution of $V_{CM,P}$ in real gearless turbines is expected to be much more pronounced.

VI. CONCLUSION

This paper presents a systematic investigation of CMV-induced bearing currents in wind turbine systems across different configurations. A unified wind turbine model is first established to enable comparative analysis between geared and gearless topologies. Based on this model, CMV propagation paths are analyzed and a system-level equivalent capacitive circuit model is developed. The BVR is then derived to quantify the contributions of generator-side and pitch-side CMVs.

Experimental and simulation studies demonstrate that both CMV sources significantly influence shaft voltage and bearing current behavior, with their relative contributions depending on turbine configuration and interface conditions. Results show that tight brush contact and conductive grease effectively suppress BVR, although dv/dt-induced current spikes remain. In contrast, brush contamination increases shaft voltage and significantly raises the probability of bearing breakdown, accompanied by high-amplitude EDM currents. The use of insulation spacers is shown to effectively reduce pitch-side CMV coupling. Furthermore, the impact of pitch-induced CMV is expected to be more pronounced in practical turbines due to higher voltage levels. These findings provide valuable insights for improving wind turbine reliability and developing targeted mitigation strategies.

ACKNOWLEDGMENT

This project is launched together with SKF, Rabbalshede Kraft, Göteborg Energi AB, ABB AB and Skellefteå Kraft. The authors sincerely acknowledge their support. They would also like to express their special thanks to Olle Bankestrom from SKF for his extensive experience in bearing current research, which provided valuable technical insights and inspiration throughout this work. They also report the use of OpenAI's ChatGPT for improving the language, grammar, and readability of the manuscript.

REFERENCES

[1] G. W. E. Council. (2026). *Global Wind Report 2026*. [Online]. Available: https://www.gwec.net/reports/globalwindreport

[2] J. Ribrant and L. M. Bertling, "Survey of failures in wind power systems with focus on Swedish wind power plants during 1997–2005," *IEEE Trans. Energy Convers.*, vol. 22, no. 1, pp. 167–173, Mar. 2007, doi: 10.1109/TEC.2006.889614.

[3] C. Su, Y. Yang, X. Wang, and Z. Hu, "Failures analysis of wind turbines: Case study of a Chinese wind farm," in *Proc. Prognostics Syst. Health Manage. Conf. (PHM-Chengdu)*, Oct. 2016, pp. 1–6, doi: 10.1109/PHM.2016.7819826.

[4] S. Yagi and N. Ninoyu, "Technical trends in wind turbine bearings," NTN Tech. Rev., Tech. Rep., 2008.

[5] C. Radu. (Mar. 2020). *The Most Common Causes of Bearing Failure and the Importance of Bearing Lubrication*. RKB Technical Review, Switzerland. [Online]. Available: https://www.bearing-news.com/the-most-common-causes-of-bearing-failure-and-the-importance-of-bearing-lubrication/

[6] N. Tazi, E. Chatelet, and Y. Bouzidi, ''Wear analysis of wind turbine bearings,'' *Int. J. Renew. Energy Res.*, vol. 7, pp. 2120–2129, Jan. 2017.
[7] B. AlikhanzadehAlamdari, G. Tekin, R. G. Sengoga, and W. Yuan, ''Causes of currents in the wind turbine bearings,'' Tech. Rep., 2017, vol. 2023, p. 2.
[8] *Rolling Bearings Damage and Failures*, Standard ISO 15243, 2017.
[9] *Rolling Bearing Failure V2*, FAG, 2005.
[10] SKF. *Bearing Damage and Failure Analysis*. [Online]. Available: https://www.skf.com/binaries/pub12/Images/0901d1968064c148-Bearing-failures---14219_2-EN_tcm_12-297619.pdf
[11] A. Muetze, ''Bearing currents in inverter-fed AC-motors,'' TU Darmstadt, Darmstadt, Germany, Tech. Rep., 2004. [Online]. Available: https://api.semanticscholar.org/CorpusID:112828069
[12] J. Zhao, X. Xu, and O. Carlson, ''Electrostatic discharge impacts on the main shaft bearings of wind turbines,'' *Wind Energy Sci.*, vol. 8, no. 12, pp. 1809–1819, Dec. 2023, doi: 10.5194/wes-8-1809-2023.
[13] Y. Gemeinder and M. Weicker, ''Application guide bearing currents_V2.3,'' Tech. Rep., 2021. [Online]. Available: https://tuprints.ulb.tu-darmstadt.de/id/eprint/19393
[14] A. Joshi, ''Electrical characterisations of bearings,'' Ph.D. thesis, 2019.
[15] O. Magdun, Y. Gemeinder, and A. Binder, ''Investigation of influence of bearing load and bearing temperature on EDM bearing currents,'' in *Proc. IEEE Energy Convers. Congr. Expo.*, Sep. 2010, pp. 2733–2738, doi: 10.1109/ECCE.2010.5618061.
[16] R. automation, ''Inverter Driven induction motors shaft bearing current solution,'' Ind. White Paper, 2002.
[17] D. Busse, J. Erdman, R. J. Kerkman, D. Schlegel, and G. Skibinski, ''Bearing currents and their relationship to PWM drives,'' *IEEE Trans. Power Electron.*, vol. 12, no. 2, pp. 243–252, Mar. 1997, doi: 10.1109/63.558735.
[18] J. Zhao, X. Xu, and O. Carlson, ''Common mode voltage impact on wind turbine main shaft bearing,'' in *Proc. 23rd Eur. Conf. Power Electron. Appl. (EPE ECCE Europe)*, Sep. 2021, pp. P.1–P.7, doi: 10.23919/EPE21ECCEEurope50061.2021.9570495.
[19] E. Hart, B. Clarke, G. Nicholas, A. Kazemi Amiri, J. Stirling, J. Carroll, R. Dwyer-Joyce, A. McDonald, and H. Long, "A review of wind turbine main bearings: Design, operation, modelling, damage mechanisms and fault detection," *Wind Energy Sci.*, vol. 5, no. 1, pp. 105–124, Jan. 2020, doi: 10.5194/wes-5-105-2020.
[20] T. García-Sánchez, I. Muñoz-Benavente, E. Gómez-Lázaro, and A. Fernández-Guillamón, ''Modelling types 1 and 2 wind turbines based on IEC 61400-27-1: Transient response under voltage dips,'' *Energies*, vol. 13, no. 16, p. 4078, Aug. 2020, doi: 10.3390/en13164078.
[21] Standard IEC 61400-27-1, 2015.
[22] Standard IEC 61400-24, 2019.
[23] A. Muetze and A. Binder, ''Generation of high-frequency common mode currents in machines of inverter-based drive systems,'' in *Proc. Eur. Conf. Power Electron. Appl.*, Sep. 2005, pp. 10 p. P.10, doi: 10.1109/epe.2005.219489.
[24] R. Boylestad, *Introductory Circuit Analysis*, 14th ed. London, U.K.: Pearson, 2023.
[25] D. R. Patrick and S. W. Fardo, ''Basics of electrical circuits,'' in *Electrical Distribution Systems*, River Publishers, 2009, ch. 2, pp. 15–40.

JIAN ZHAO received the M.S. degree in electrical engineering from Harbin Institute of Technology, Harbin, China, in 2013. He is currently pursuing the Ph.D. degree in electric power engineering with the Chalmers University of Technology, Gothenburg, Sweden. After graduation, he worked in the industrial automation and electric vehicle industries, gaining hands-on experience in the design and manufacturing of electrical machines, as well as optimizing their integration into complex systems. His current research focuses on bearing currents in wind turbine systems, particularly related to power electronics and electrostatic field issues within the wind turbine. His research interests include electrical machine analyzation, power electronics, and their integration into renewable energy systems and electric vehicles.

XIAOFEI LEI received the M.S. degree in electrical engineering from Harbin Institute of Technology, Harbin, China, in 2013. She is currently a Lecturer with the Department of Electronic and Information Engineering, Hulunbuir University, Hulunbuir, China. Since joining the university, she has been actively involved in both teaching and research. Her academic and research interests include a wide range of interdisciplinary fields, including power electronics, electric machine systems, inertial energy storage technologies, and wind power generation. In recent years, her work has also extended to applied research in agricultural Internet of Things (IoT), as well as remote sensing and image processing techniques for monitoring grassland ecosystems. Her research contributes to the development and application of green energy technologies, with a focus on enhancing the efficiency, sustainability, and regional adaptability of renewable energy systems.

XULIANG ZHU received the B.S. degree in electrical engineering and automation from Yanshan University, Qinhuangdao, China, in 2011. He is currently an Electrical Engineer with CGN (Guizhou) New Energy Company Ltd. He has accumulated more than 13 years of professional experience in the wind power industry. Since graduation, he has been extensively involved in the installation, commissioning, and operational management of over 200 wind turbine units. His areas of expertise include the operation and maintenance of DFIG wind turbines, performance assessment, and the diagnosis and resolution of complex system faults. His current work focuses on enhancing the reliability and operational efficiency of wind energy systems.

KEFEI ZHU received the B.S. degree in mechanical engineering from Harbin Institute of Technology, China, in 2010, and the Ph.D. degree from Hanyang University, Republic of Korea, in 2016. Currently, he is a Senior Engineer working on electric motor and bearing engineering field. His research interests include electric motor design, noise and vibration analysis of electric motor and bearing, bearing fault analysis due to shaft current, intelligent monitor, and diagnosis of bearing.

OLA CARLSON was born in Onsala, Sweden, in 1955. He received the M.Sc. and Ph.D. degrees in electrical engineering from the Chalmers University of Technology, Gothenburg, Sweden, in 1980 and 1988, respectively. He is currently a Professor with the Department of Electrical Engineering, Chalmers University of Technology. His major interests include electrical systems for renewable power production, especially wind power, smart grids, and hybrid electric vehicles.